Catalysis Today 476 (2026) 115898

Contents lists available at ScienceDirect

Catalysis Today

journal homepage: www.elsevier.com/locate/cattod

Integrated VOCs abatement and CO_2 valorization: Capture and solar fuels production over sustainable materials☆

Roberto Fiorenza [a,*], Martina Salzano De Luna [b], Mariano Sirignano [b], Luigi Carbone [c,d], Riccardo Scarfiello [c,d], Giusy Dativo [a], Luca Calantropo [a], Marianna Bellardita [e]

[a] Department of Chemical Sciences, University of Catania, Viale A. Doria 6, Catania 95125, Italy
[b] Department of Chemical, Materials and Industrial Production Engineering, University of Naples Federico II, Piazzale V. Tecchio 80, Napoli 80125, Italy
[c] CNR NANOTEC - Institute of Nanotechnology, c/o Campus Ecotekne University of Salento, Via Monteroni, Lecce 73100, Italy
[d] Istituto Italiano di Tecnologia, Center for Biomolecular Nanotechnologies, Arnesano, LE 73010, Italy
[e] Engineering Department, University of Palermo, Viale delle Scienze, Ed. 6, Palermo 90128, Italy

ARTICLE INFO

Keywords:
VOCs removal
CO_2conversion
CO_2capture
Photothermo-catalysis
Noble metals-free catalysts
Cryogels

ABSTRACT

The management of the CO_2 produced during the catalytic oxidation of volatile organic compounds (VOCs) is a key challenge for the development of sustainable air purification processes. In this work, an integrated approach was investigated, where the CO_2 evolved by the catalytic oxidation of toluene, used as a model VOC, was either captured by sustainable zeolite-based cryogels or straightforwardly converted into solar fuels through a photothermo-catalytic route. For the CO_2 capture, chitosan/poly(ethylene glycol) diglycidyl ether cryogels containing zeolite 13X were prepared. The presence of zeolite strongly improved the adsorption performance, allowing a capture efficiency of about 70% in the integrated test, whereas a negligible CO_2 uptake was obtained with the cryogel without zeolite. For the CO_2 conversion, 1 wt% Cu_2O-TiO_2 supported on Ni/Ce-modified phyllosilicates was examined. Among the investigated samples, the modified kaolinite support showed the best performance, reaching 77% of CO_2 conversion after 4 h of solar photothermo-catalytic test at 120 °C. The improved activity of this sample was mainly related to the higher amount of basic sites, especially those with medium strength, favouring the adsorption and activation of CO_2, whereas the Cu_2O-TiO_2 mixed oxide promoted the photocatalytic contribution under simulated solar irradiation. The integrated strategy here proposed is promising to couple VOC removal with CO_2 capture/utilization using sustainable materials, thus contributing to a circular approach for environmental protection.

1. Introduction

Air quality in both indoor and outdoor environments is a major current concern. In particular, the removal of volatile organic compounds (VOCs) and CO_2 management are critical issues and are directly/indirectly related to several of the 17 Sustainable Development Goals (SDGs) of the United Nations. In particular: SDG 7: affordable and clean energy, SDG 11: sustainable cities and communities, SDG 12: responsible consumption and production and SDG 13: climate action [1].

Among the various technologies for the VOCs removal, the catalytic oxidation is one of the most widely used, because it enables the complete mineralization of VOCs under milder conditions, compared to the non-catalytic combustion methods, allowing also the treatment of different VOCs over a broad concentration range [2]. However, the produced CO_2 must be addressed.

In this context, we originally proposed an integrated approach, in which the CO_2 produced from the thermal catalytic oxidation of VOCs can either be captured with sustainable cryogels or converted into solar fuels by noble metals-free catalysts through a solar photothermo-catalytic route.

Regarding the first approach, we have developed cryogels in which zeolite particles, which are well known for their reversible CO_2 adsorption capability, are embedded within and held together by a biopolymeric framework composed of chitosan and poly(ethylene

☆ This work is dedicated to the memory of Prof. Carmelo Crisafulli (University of Catania), who inspired and co-founded the Laboratory of Industrial and Environmental Catalysis at the Department of Chemical Sciences in Catania. His vision and contributions made this research possible.

* Corresponding author.
E-mail address: rfiorenza@unict.it (R. Fiorenza).

https://doi.org/10.1016/j.cattod.2026.115898
Received 24 April 2026; Received in revised form 11 June 2026; Accepted 22 June 2026
Available online 26 June 2026
0920-5861/© 2026 The Authors. Published by Elsevier B.V. This is an open access article under the CC BY license (http://creativecommons.org/licenses/by/4.0/).

glycol) diglycidyl ether as a crosslinking agent. In this way, high-performance monolithic adsorbents can be obtained, overcoming the typical technological limitation of zeolites associated with their powdery form [3–5].

Whereas for the CO_2 conversion approach, the application of hybrid catalysis, such as the photothermo-catalysis, allowed to exploit an energy-saving and efficient process compared to both the energy-intensive thermocatalytic CO_2 conversion reaction and the photocatalytic route at room temperature, which is characterized by very low yields into solar fuels [6–8].

In the present work, for the solar photothermo-catalytic conversion of CO_2, arising from the toluene (VOC model) catalytic oxidation, we investigated the performance of a noble metal-free composite supported on modified phyllosilicates. In particular, we studied the performance of 1 wt% Cu_2O-TiO_2, which permits the efficient exploitation of the photocatalytic properties of TiO_2 enhanced by the presence of cuprous oxide that acts as an electron donor for the CO_2 reduction reaction [9,10]. The physicochemical properties of this composite and the beneficial role of copper species have been extensively investigated in our previous studies, including their interaction with CeO_2, Co-based species, zeolites, and different TiO_2 crystalline phases [8,9,11].

The Cu_2O-TiO_2 mixed oxide was supported on different phyllosilicates (mordenite, kaolinite, halloysite and sepiolite) modified by the intercalation of Ni and Ce. This chemical treatment increased the CO_2 adsorption on the basic sites of the phyllosilicates, allowed the exploitation of the thermally activated redox properties of Ce ions, and efficiently promoted the thermocatalytic CO_2 activation by Ni [6,7], thus enabling a holistic effect that combines these thermocatalytic features with the photocatalytic ones of the Cu_2O-TiO_2.

Therefore, we propose an integrated approach that combines CO_2 capture and solar-driven photothermo-catalytic conversion over sustainable materials, directly applied to the gas stream of the toluene catalytic oxidation. By coupling air pollutant abatement with CO_2 valorization by capture or by conversion into high added-value solar fuels, the here investigated process establishes a circular pathway toward improved environmental sustainability.

2. Materials and Methods

2.1. Sample preparation

Chemically crosslinked chitosan-based cryogels were prepared by modifying the procedure previously reported in the ref. [12] with the aim of (i) chemically crosslinking the polymeric framework to improve cryogel stability and (ii) inducing a finer microstructure by adjusting the temperature selected for the freeze-casting process.

Chitosan (CS) powder (molecular weight: 190–310 kDa; deacetylation degree 75–85%, by Sigma Aldrich) was dissolved in a 2 vol% aqueous acetic acid solution under stirring at room temperature for about 24 h. The pH of the CS solution (20 mg/mL) was ~3.8. Poly (ethylene glycol) diglycidyl ether (PEGDGE, average M_n 500, by Sigma Aldrich) was used as crosslinker [13]. It was added dropwise to the CS solution (CS/PEGDGE weight ratio of 1/1) under stirring at room temperature. Then, Zeolite 13X powder (ZX, average particle size 2 μm, by Sigma Aldrich) was added to the CS/PEGDGE solution (polymer/ZX weight ratio of 1/4) and mechanically stirred to get a homogeneous mixture. The latter was finally poured into cylindrical plastic tubes and rapidly frozen by immersion in liquid nitrogen. After storing the samples for one week in a freezer at −25 °C, macroporous cryogels were obtained by lyophilization.

The 1 wt% Cu_2O-TiO_2 composite was prepared following the procedure previously reported [9]. The amount of cuprous oxide (1 wt%) was the optimal one to favour the CO_2 reduction reaction under similar reaction conditions of this work and to ensure strong interaction with the TiO_2 [8,9].

In particular, the stoichiometric aqueous solution of copper (II) chloride was added to the TiO_2 (Aeroxide® P25) under stirring at 55 °C in a water bath. Subsequently, 10 mL of 2 M NaOH solution was further added, and the resulting dispersion was stirred for 30 min. Afterwards, 10 mL of ascorbic acid solution (0.5 M), used as a reducing agent, were added, and the obtained dispersion was stirred for further 3 h. Finally, the obtained slurry was centrifuged at 9000 rpm for 10 min and washed with deionized water several times. The obtained powders were dried at 55 °C under vacuum overnight.

The intercalation of Ni and Ce into the examined phyllosilicates Montmorillonite K30 (Sigma-Aldrich 69904); Kaolinite (Sigma-Aldrich 03584); Halloysite nanoclay (Sigma-Aldrich 685445); Sepiolite (Sigma-Aldrich 70253) was carried out following the procedures reported in the ref. [6]. In detail, 0.8 g of phyllosilicates were dispersed in 50 mL of a 50:50 acetone-water solution and maintained at 50 °C for 24 h. Afterwards, two aqueous solutions of 3.0 g of $Ce(NO_3)_3$•$6H_2O$ in 40 mL of water and the other containing 2.0 g of $Ni(NO_3)_2$•6 H_2O in 40 mL of water, were added to the phyllosilicate solution and stirred at 50 °C for 24 h. The resulting mixture was dried at 80 °C for 24 h and then calcined at 300 °C for 2 h.

Finally, the 1 wt% Cu_2O-TiO_2/phyllosilicate composites were synthesized with a modified solid-state dispersion (SSD) method [9,14] followed by a hydrothermal treatment. Specifically, 200 mg of Ni-Ce/phyllosilicates and 200 mg of 1 wt% Cu_2O-TiO_2 were homogeneously mixed with a pestle into an alumina mortar. The resulting powder mixture was transferred to a beaker containing 30 mL of deionized water and sonicated for 30 min. The suspension was then placed in a Teflon-lined autoclave and heated at 80 °C for 5 h. Subsequently, the product was centrifuged at 9000 rpm three times, and the obtained solids were dried at room temperature for 24 h.

These samples are coded as 1CuTi/ phyllosilicates, where MON = montmorillonite, KAO = kaolinite, HAL = halloysite and SEP = sepiolite.

2.2. Cryogels characterizations

The microstructure of the produced cryogels was investigated by scanning electron microscopy (SEM) with a Tescan CLARA microscope. The observations were performed on samples previously cut with a razor blade and sputter-coated with an Au layer.

Carbon dioxide equilibrium adsorption isotherms were recorded at 25 °C with a 3Flex apparatus by Micromeritics. Before each test, the samples were activated at 150 °C under nitrogen flow for 12 h using the FlowPrep 060 Sample Degas System by Micromeritics.

The sample stability at 150 °C was previously assessed by thermogravimetric analyses carried out using a TGA Q500 (TA Instruments). Samples were heated from room temperature up to 700 °C at a rate of 10 °C/min under a nitrogen atmosphere. The analyses allowed the determination of the thermal stability window of the cryogels and the actual polymer/zeolite weight ratio.

2.3. 1%Cu_2O-TiO_2 supported on the modified phyllosilicates characterizations

The FTIR spectra were recorded with a Spectrum Two System (Perkin Elmer), using KBr powders as reference.

The textural properties of the photothermo-catalysts were evaluated by N_2 adsorption-desorption measurements with an ASAP 2000 instrument, outgassing the samples overnight at 120 °C. The surface area was determined by the Brunauer-Emmett-Teller (BET) method in the standard pressure range 0.05–0.3 p/p_0. The pore volume and pore size distribution were evaluated by analysis of the desorption curve, using the Barrett, Joyner, and Halenda (BJH) method.

The UV–vis Diffuse Reflectance Spectroscopy (DRS) spectra were recorded with a JASCO V−670. The optical band-gap of the samples (E_g) was evaluated by plotting the modified Kubelka–Munk function vs the $h\nu$, using $BaSO_4$ as reference [15]. It is important to highlight that the

application of this method to composite materials requires some additional considerations. As reported in refs. [15,16] in fact, the reflectance spectra of these samples are more complex than those of bare semiconductor oxides with a homogeneous crystalline phase, because of the absorption from the impurity phases present in this type of complex composites. Therefore, to extrapolate the E_g values, these features were also considered.

The CO_2-TPD (Temperature Programmed Desorption) measurements were carried out in a fixed-bed quartz reactor filled with 150 mg of sample. After the adsorption and surface saturation process, the CO_2 flow (30 cc/min) was stopped. Afterwards, the reactor was heated from 30 °C to 500 °C (rate of 10 °C/min). The CO_2 desorption peaks were acquired with a mass spectrometer (Sensorlab VG Quadrupoles). Before the measurements, the samples were pre-treated with a He flow (30 cc/min) overnight at 150 °C.

X-ray photoelectron spectroscopy analysis (XPS) was performed with a K-Alpha™ + X-ray photoelectron spectrometer. The binding energy of the C (1 s) peak at 284.9 eV (relative to adventitious carbon) was employed as a reference.

SEM-EDX analysis was carried out with a ZEISS SUPRA 55 VP equipped with an energy dispersive X-ray (EDX) INCA-Oxford windowless detector.

The photoluminescence (PL) spectra were acquired using a Perkin Elmer LS45 luminescence Spectrometry apparatus with an excitation λ of 300 nm.

2.4. CO_2 capture/conversion from the catalytic oxidation of VOC

The employed experimental set-up is illustrated in the supporting information (Fig. S1). In particular, the catalytic oxidation of toluene (used as a model VOC) was carried out in a heated flow reactor. The reaction was performed continuously at atmospheric pressure using 150 mg of 1 wt% Au/CeO_2 catalyst, chosen as the best catalyst, under our experimental conditions, to favour the total oxidation of toluene into CO_2, adopting the same experimental procedures and the sample preparation method reported previously [17]. The reactor was heated with a programmable oven with a heating rate of 10 °C/min from 30 °C to 310 °C, the temperature at which the total combustion of toluene was verified (Fig. S2) and was maintained at this temperature (310 °C) for the entire duration of the integrated approach tests.

Before the measurements, the reactant mixture (0.7 vol% toluene; 10 vol% air, balance in He) was adsorbed–desorbed over the 1%Au/CeO_2 catalyst for 30 min to assure steady-state conditions. With this procedure, conversion and selectivity were reproducible within 3–5%. Preliminary runs performed at different flow rates demonstrated the absence of external diffusional limitations. The absence of internal diffusion limitations was instead verified by running experiments with different powder grain sizes. We excluded the occurrence of heat transfer limitations because we found that the temperature of the reactor at different heights was substantially the same, reasonably due to the low concentration of the reactants used in the catalytic tests. The flow rate of the reactants mixture was 60 cc/min. The effluent gases were examined on-line by a gas chromatograph, equipped with a packed column with 10% FFAP on ChromosorbW and an FID detector, and by a quadrupole mass spectrometer (VG Quadrupoles). The carbon balance was always higher than 95%.

The evolved CO_2 was continuously fed into a tubular Pyrex photoreactor (Fig. S1), filled with 200 mg of as-prepared cryogels for the CO_2 capture or with the 1 wt% Cu_2O-TiO_2 supported on Ni/Ce-phyllosilicates for the photothermo-catalytic CO_2 conversion. These latter samples were therefore irradiated for 4 h with a solar lamp (Osram Ultra Vitalux 300 W, irradiance of 10.7 mW/cm^2) and the tubular reactor was surrounded by aluminium foils in order to reach a temperature of 120 °C, accurately controlled by an infrared thermal camera. For both reactions, the CO_2 conversion values, or the CO_2 capture percentages, were evaluated using an Agilent 8860 gas chromatograph (Carboxen−1000 column, TCD detector) calibrated for the detection of carbon dioxide, methane, and carbon monoxide, and with the Trace GC instrument (Porapak Q column, FID detector) used to detect the possible formation of other organic compounds.

The CO_2 conversion/capture values were determined after 4 h of reaction with the following equation:

CO_2 conversion/capture (%):

$$\left(\frac{\mathrm{Area}_{\text{peak CO2in}} - \mathrm{Area}_{\text{peak CO2out}} \times \left(\frac{\mathrm{Area}_{\text{peak standard in}}}{\mathrm{Area}_{\text{peak standard out}}}\right)}{\mathrm{Area}_{\text{peakCO2in}}}\right) \times 100$$

Furthermore, the mass balance method was applied, considering the following equation:

CO_2 conversion/capture (%):

$$\left(\frac{\mathrm{Area}_{\text{peak CO2out}}}{\mathrm{Area}_{\text{peak products out}} + \mathrm{Area}_{\text{peak CO2out}}}\right) \times 100$$

The two methods were in agreement with each other (± 5%, reproducibility 95%).

The values of the CO_2 conversion and of the CO_2 capture were also evaluated following the signal $m/z = 44$ of the connected GC-MS, opportunely calibrated, and the values were in agreement with each other (± 5%, reproducibility 95%).

For the solar photothermo-catalytic CO_2 conversion, the molar selectivity towards CO and CH_4 products was evaluated with Equations 1 and 2:

$$\text{CH}_4 \text{ selectivity \% : } \left(\frac{N_{CH4}}{(N_{CH4} + N_{CO})}\right) \times 100 \quad (1)$$

$$\text{CO selectivity \% : } \left(\frac{N_{CO}}{(N_{CH4} + N_{CO})}\right) \times 100 \quad (2)$$

where N_{CH4} and N_{CO} are the production rates of CH_4 and CO in μmol/$g_{catalyst} \bullet h_{irradiation}$.

Before the tests the samples for the CO_2 capture were treated under He flow (30 cc/min) overnight at 150 °C, whereas the phyllosilicates-based composites were subjected to surface cleaning by irradiation with an UV lamp under He flow following the procedure reported in the literature [8,18,19], to avoid possible interferences due to the presence of carbonaceous contaminants on the sample surface.

3. Results and discussion

3.1. Cryogels-materials characterizations and CO_2 isotherms

The microstructure of the cryogels is shown in the SEM micrographs reported in Fig. 1. The CS/PEGDGE sample exhibits the representative microstructure of cryogels, characterize by a thin polymeric walls and large pores (on the order of tens of micrometres) formed during the

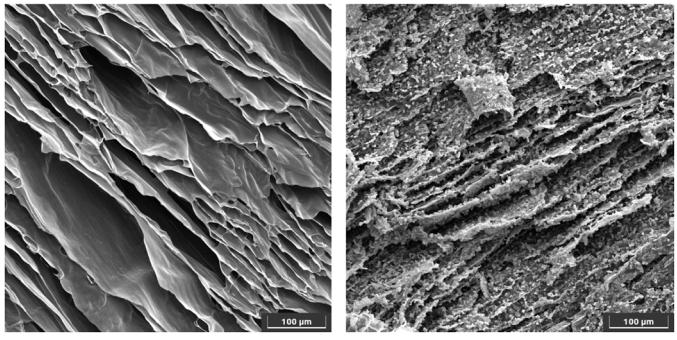


Fig. 1. SEM micrographs of CS/PEGDGE (left) and CS/PEGDGE + ZX (right) cryogels.

freeze-casting process. In the CS/PEGDGE + ZX sample, the cryogel appears to be more compact, and the zeolite particles are uniformly dispersed on and within the polymeric walls.

Due to the presence of the polymeric binder "gluing" together zeolite particles, thermogravimetric analyses were carried out before performing any thermal treatment to determine the actual stability window of the cryogels (Fig. 2).

For the CS/PEGDGE sample, the weight change up to around 100 °C can be ascribed to the loss of adsorbed water, while changes at higher temperatures are due to thermal degradation of the polymeric network. In the presence of zeolite, the weight loss due to water extends up to around 200 °C, as water molecules are more strongly retained in the zeolite-containing sample and therefore require more energy to be released. Moreover, the shoulder at around 240 °C in the thermogram of the CS/PEGDGE + ZX sample corresponds to the onset of thermal degradation processes involving the polymer phase. For this reason, activation of the samples prior to adsorption experiments was carried out well below this threshold temperature, namely at 150 °C, to avoid any degradation of the polymer phase.

The results of the CO_2 equilibrium adsorption experiments, using pure CO_2 gas stream, are shown in Fig. 3, in which the adsorbed CO_2 amount (q_e) is plotted as a function of the gas pressure at equilibrium.

Since the CO_2 adsorption capacity of the pure CS/PEGDGE cryogels is extremely low, the CO_2 uptake of the CS/PEGDGE + ZX sample can be mainly ascribed to the presence of zeolite particles embedded into the polymeric framework. The adsorption behavior can be satisfactorily described by the Langmuir model [20], leading to a maximum CO_2 adsorption capacity value of about 2.48 mmol/g.

3.2. CO_2 capture from the integrated approach

The same adsorbents were used in the integrated approach (CO_2 coming from the toluene catalytic oxidation) in order to evaluate the CO_2 capture percentage after 4 h of this test. As expected from the CO_2 adsorption isotherms reported in Fig. 3, the CS/PEGDGE cryogel is unable to capture relevant amounts of CO_2 under the dynamic conditions generated by the catalytic toluene oxidation process. In contrast, the CS/PEGDGE + ZX cryogel is able to capture a substantial fraction of the carbon dioxide produced over 4 h of toluene oxidation, reaching a capture efficiency of 69.5%. It should be noted that the potential maximum adsorption capacity might be not fully exploited under the flow conditions at the outlet of the catalytic reactor, likely because of kinetic and/or residence-time limitations. In particular, the relatively short residence time of the gas stream and possible mass-transfer limitations at the outlet of the catalytic reactor may hinder the full exploitation of the equilibrium adsorption capacity under dynamic conditions. Therefore, a lower flow rate could be adopted to further exploit the CO_2 adsorption capacity of the CS/PEGDGE + ZX cryogel, leading to even higher capture efficiency values.

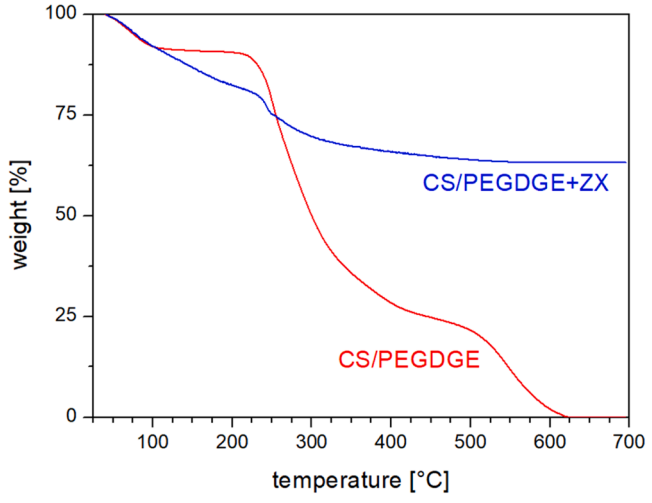


Fig. 2. TGA curves for CS/PEGDGE and CS/PEGDGE + ZX cryogels.

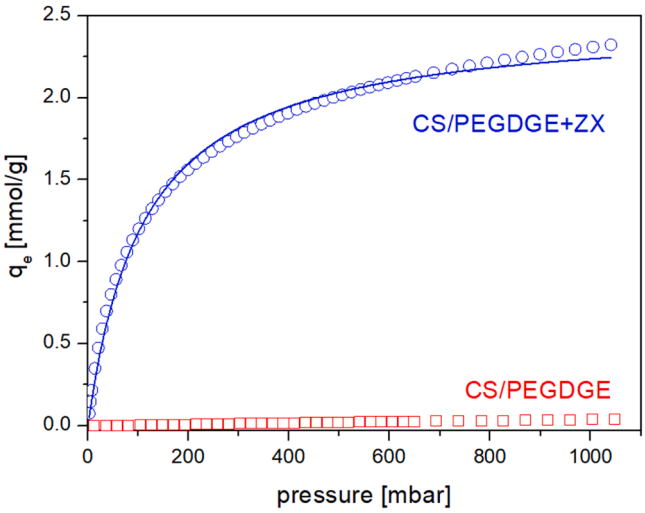


Fig. 3. CO_2 adsorption isotherms of CS/PEGDGE and CS/PEGDGE + ZX cryogels. The solid line represents the best fit of the Langmuir model to experimental data.

Furthermore, it is important to underline that, in the integrated approach, the material was tested under a significantly more complex gas composition than that employed in the CO_2 adsorption isotherm tests, which were carried out using a pure CO_2 stream (Fig. 3). Indeed, the gas stream generated by toluene oxidation contains not only CO_2 but also air, water vapor, and possible traces of reaction by-products. Therefore, the performances measured in the integrated configuration should be considered net values obtained under multicomponent operating conditions. Under this environment, competitive adsorption of H_2O on the hydrophilic zeolite-based cryogel may partially reduce the availability of adsorption sites for CO_2, thereby affecting the observed capture efficiency in the integrated test.

3.3. Solar photothermo-catalytic CO_2 conversion using the integrated approach

The performances of the 1 wt% Cu_2O/TiO_2 composite supported on the Ni/Ce-intercalated phyllosilicates in the CO_2 conversion arising from the catalytic oxidation of toluene are reported in Table 1. In our experimental conditions, only CO and CH_4 were detected as solar fuels [7,8]. For all the samples, the CO was the main product with some formation of CH_4, pointing to a preferential two-electron reduction pathway [11,21]. Notably, the addition of the modified phyllosilicates promoted the CO_2 reduction reaction compared to the bare 1CuTi.

Interestingly, among the tested supports, the Ni/Ce-kaolinite sample gave the best results with the 77% CO_2 conversion arising from the catalytic oxidation of toluene. Conversely, the interaction of the 1% Cu_2O/TiO_2 with the modified sepiolite did not provide substantial improvements compared to the unsupported 1CuTi. It is also important to highlight that the hybrid solar photothermo-catalytic approach is essential to obtain this activity at relatively low temperature (120 °C). Indeed, even using the 1CuTi/KAO catalyst, no CO_2 conversion was detected in the bare solar photocatalytic test at room temperature, whereas in the dark thermocatalytic tests, a CO_2 conversion of 55% was reached only at 200 °C, with no measurable activity observed at lower temperatures, including 120 °C. These findings highlight the synergistic effect of simulated solar light in assisting the catalytic mechanism [7,8,22,23], resulting in an activity at low temperature, that was higher than the sum of the single photocatalytic and thermocatalytic approaches,

Table 1
Solar photothermo-catalytic parameters after 4 h of CO_2 conversion reaction at 120 °C.

Sample	CO_2 conversion (%)	CO formation rate (μmol/g•h)	CH_4 formation rate (μmol/g•h)	CO selectivity (%)	CH_4 selectivity (%)
1CuTi/MON	59	16	6	73	27
1CuTi/SEP	23	6	/	100	/
1CuTi/HAL	55	15	4	79	21
1CuTi/KAO	77	21	9	70	30
1CuTi	19	5	/	100	/

with the additional benefit of reduced energy demand.

Figure S3 shows the solar photothermo-catalytic stability of the 1CuTi/KAO catalyst during 25-h continuous test performed at 120 °C. After 15 h of operation, the CO_2 conversion decreased by approximately 7%. Thereafter, only a slight additional decline was observed, with the catalyst maintaining a CO_2 conversion of about 68% after 25 h on stream. Overall, the loss of catalytic activity was limited to approximately 10%, indicating good stability under the adopted reaction conditions. The observed decrease may be related to the continuous exposure of the catalyst to the complex gas stream generated during toluene oxidation, containing CO_2, air, water vapor, and possible traces of reaction by-products, which may progressively affect the efficiency of the CO_2 reduction process.

In order to rationalize the observed differences in photothermo-catalytic activity, the prepared composites were systematically characterized.

Fig. 4 reports the FT-IR spectra of the analysed composites. All the catalysts showed wide bands centred in the range 3700–3350 cm^{-1} related to the O-H stretching of the phyllosilicate supports. In particular, the 1CuTi/KAO and 1CuTi/HAL showed two bands in the range 3700–3600 cm^{-1} associated with the presence of Al in their structure, which gives rise to the formation of the stretching vibration of the inner-surface Al–OH groups [24]. The O-H bending was detected for all the samples in the range 1631–1600 cm^{-1}, and it is also related to the O-H groups present in the layers of the phyllosilicates due to the water adsorbed/intercalated in the structures [25]. The wide bands at 1045–1020 cm^{-1} are typical of the stretching vibration of the Si-O-Si bonds, whereas the bending vibration is in the 915–900 cm^{-1} interval [24–26]. In the 1CuTi/KAO sample, additional bands at about 1108 and 1004 cm^{-1} are due to mono-substituted Si-O stretching [26]. Finally, the bands at low wavenumbers (< 700 cm^{-1}) were associated with the M-O bonds (M= Metal as Ni, Ce, Ti, Cu) [6,9]. Interestingly, only the 1CuTi/KAO sample (the best one in the photothermo-catalytic CO_2 conversion, Table 1) showed a little band at about 1355 cm^{-1} attributed to the symmetric vibration of carboxylate groups (COO^-) formed from the interaction of the phyllosilicate-based samples with the atmospheric CO_2 [27]. The other composites showed instead a negative feature likely associated with the desorption of physisorbed CO_2 (Fig. 4) [28], indicating that only with the modified kaolinite, even with the atmospheric CO_2, the interaction with its basic sites led to the formation of weak bonds. Therefore, in this sample, the CO_2 adsorption/activation appears to be favoured.

To verify the key contribution on the reaction to the presence of basic sites and their effects on the CO_2 adsorption/activation, Fig. 5 reports the CO_2-TPD profiles of the investigated samples. To correlate the basic features of the examined composites with the photothermo-catalytic activity, we also recorded the profile of the unsupported 1CuTi sample.

The CO_2-TPD profiles can be divided into three zones considering the type of the basic sites: α for weak (CO_2 desorption peaks from 30 to 140 °C), β for medium (CO_2 desorption peaks from 140 to 450 °C), and γ for strong (CO_2 desorption peaks above 450 °C) basic sites [29]. For the CO_2 conversion reaction, it is important to highlight that it is important to exploit basic sites that are neither too strong nor too weak. In fact, the CO_2 adsorbed on too weak basic sites cannot be activated, being favoured its desorption; on the contrary, the CO_2 adsorbed in the very strong basic sites formed stable carbonates species on the surface, difficult to be activated/converted [6,30,31].

All the composites showed a CO_2-TPD peak centred between 55 °C and 65 °C related to the presence of weak basic sites due to the interaction between surface -OH groups and the CO_2 [32]. Interestingly, the trend in the amount and distribution of basic sites follows the photothermo-catalytic activity (Table 1 and Table 2). Indeed, the 1CuTi/KAO showed the highest total amount of basic sites, with also the highest percentage of medium sites (91%), in a temperature range (158–195°C, Table 2, Fig. 5) relatively close to the operating temperature reached during the photothermo-catalytic tests (120 °C). The presence of these medium sites, as for the β sites of the other samples, is associated with CO_2 desorption from metal-oxygen pairs (M^{n+}-O^{2-} sites) [31,33] and it is particularly favourable in the 1CuTi/KAO sample to efficiently activate the CO_2 and to promote its conversion into solar fuels. The 1CuTi/MON and 1CuTi/HAL, that exhibited about 20% lower CO_2 conversion compared to 1CuTi/KAO (Table 1), also showed about

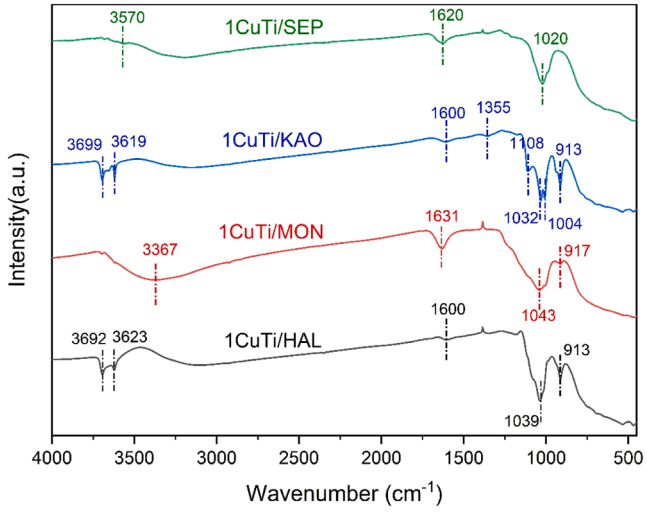


Fig. 4. FTIR spectra of the examined samples.

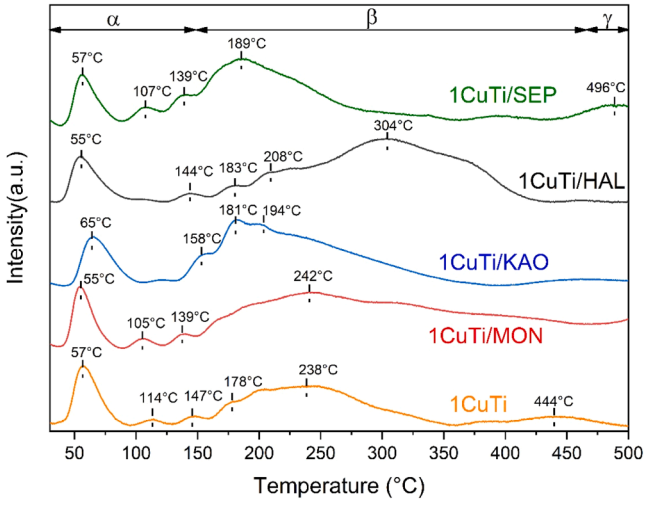


Fig. 5. CO_2-TPD profiles of the examined samples.

Table 2
Quantitative analysis of basic sites for the examined materials. α: weak (T < 140 ∘C); β: medium (140 ∘C<T < 450 ∘C); γ: strong (T > 450 ∘C) basic sites; TA_{BS}: total amount of basic sites in mmol CO_2/g_{cat}.

Sample	Basic sites			
	α (%)	β (%)	γ (%)	TA_{BS}
1CuTi/MON	11.0	89.0	/	0.32
1CuTi/SEP	20.3	70.6	9.1	0.21
1CuTi/HAL	13.6	86.4	/	0.35
1CuTi/KAO	9.4	90.6	/	0.52
1CuTi	21.9	78.1	/	0.16

0.32 and 0.35 mmol CO_2 g_{cat}^{-1} of total amount of basic sites respectively, lower compared to 1CuTi/KAO (0.56 mmol CO_2 g_{cat}^{-1}, Table 2), with some medium sites shifted at temperatures higher than 200 °C (i.e., stronger CO_2 adsorption-lower CO_2 activation, Fig. 5). This is reasonably one of the key features explaining their lower photothermo-catalytic activity compared to the 1CuTi/KAO. Consequently, the 1CuTi/SEP and 1CuTi samples displaying the lowest amount of basic sites together with the presence of strong γ sites (or high temperature β sites) that led difficult the activation and then the conversion of CO_2. Moreover, they holding the highest % of weak basic sites (20–22%) where the CO_2 desorption was favoured instead of its conversion. Indeed, these samples were the least active among the tested composites (Table 1).

The textural properties of the samples are reported in Table 3 and in Fig. 6. All the examined composites showed type IV/V isotherms with a hysteresis loop typical of the mesoporous materials [34]. In particular, the 1CuTi/HAL showed the highest surface area (128 m^2/g) and the lowest mean pore diameter and volume with a H1 hysteresis loop (Fig. 6A) associated with narrow and uniform mesopores [31,34] as also displayed in the pore size distribution curve (Fig. 6B). On the contrary, the other samples showed wider pore size distributions with a H2 hysteresis loop (Fig. 6A) typical of pores with narrow necks and wide bodies ("ink bottle" pores) [34]. These textural differences are strictly correlated to the typical morphology of the examined commercial phyllosilicates, with the halloysite nanoclay characterized by the presence of nanotubes in its structure, as largely reported in the literature, which leads to a higher exposed surface area compared to the other phyllosilicates [24,31].

The UV-DRS spectra of the examined compounds are reported in Fig. S4. All the samples showed a similar reflectance spectrum, with the main contribution, as expected, arising from the presence of TiO_2, with the typical decrease of R% at about 388 nm. Furthermore, a feature in the 500–700 nm region can be associated with interfacial charge transfer from the valence band of TiO_2 to the Cu_2O co-catalyst [8,9,35]. Consequently, no variation was detected in the optical band gap (E_g) values evaluated by the modified Kubelka-Munk function (Table 3, Fig. S3) among the analysed samples, indicating that the optical response is mainly dominated by TiO_2.

Although the 1CuTi/HAL showed the same E_g value as 1CuTi/KAO with a higher surface area (Table 3, 128 m^2/g instead of 119 m^2/g of the modified kaolinite-supported composite), it was less efficient in the CO_2 photothermo-catalytic conversion reaction than the 1CuTi/KAO (Table 1). This indicates that the greater abundance of medium basic sites (Table 2) resulting in a more favourable CO_2 activation on the modified kaolinite support. This is a more relevant factor for achieving high solar fuels production than the textural and optical properties differences alone. A high concentration of intermediate strength basic sites in the modified kaolinite facilitates the CO_2 adsorption. Subsequently, CO_2 is likely activated through a synergistic photothermo-catalytic pathway in which the intercalated Ni and Ce species contribute to its thermal/redox activation. In this system, TiO_2 acts as the primary photoactive semiconductor generating e^-/h^+ pairs under simulated solar irradiation, whereas Cu_2O enhances charge separation and facilitates electrons transfer toward adsorbed CO_2 species, thereby improving the efficiency of the CO_2 conversion into CO and CH_4 [8,9,11,36]. The predominance of CO (Table 1) suggests that CO_2 reduction mainly proceeds through a two-electron transfer process, while the lower CH_4 production indicates that subsequent multi-electron hydrogenation steps occur to a more limited extent. Overall, these results indicate that the photothermo-catalytic performance is more strictly governed by the amount and nature of the accessible basic sites of the support, especially medium basic sites, favouring the CO_2 adsorption/activation.

To verify the presence of the cuprous oxide species on the best performing sample (1CuTi/KAO), the XPS analysis was performed (Fig. S5).

Table 3
Textural and optical properties of the examined photothermo-catalysts.

Sample	BET surface area (m^2/g)	Mean pore diameter (nm)	Pore volume (cm^3/g)	E_g (eV)
1CuTi/MON	113	10	0.19	3.3
1CuTi/SEP	103	11	0.22	3.3
1CuTi/HAL	128	6	0.16	3.3
1CuTi/KAO	119	8	0.18	3.3

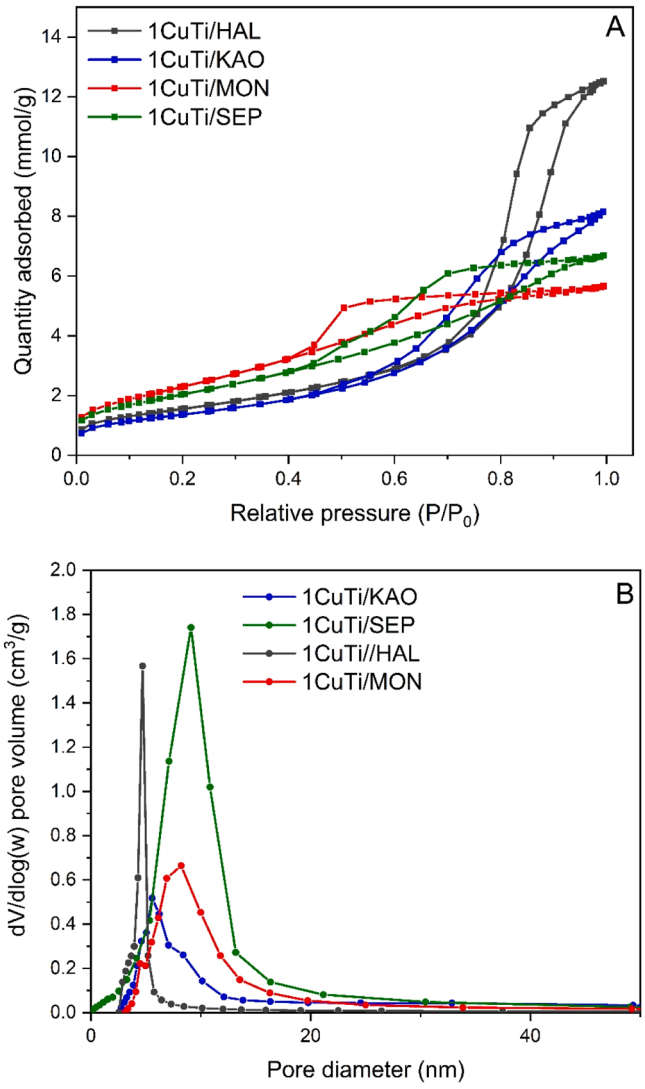


Fig. 6. N_2 adsorption-desorption curves (A) and Barrett-Joyner-Halenda (BJH) pore size distribution (B, desorption curve) of the examined photothermo-catalysts.

The Ni 2p region (Fig. S5A) exhibited the spin-orbit splitting related to Ni $2p_{3/2}$ and Ni $2p_{1/2}$. These signals are related to Ni(II) with a shake-up at ca. 6 eV. The position of the Ni $2p_{3/2}$ at about 855.2 eV suggests a strong interaction involving Ni species and the surrounding matrix/support [37]. Ce 3 d was split into eight components ascribed to several Ce 4 f level occupancies in the final state [38]. Six of these components (Fig. S5A, olive line) are assigned to Ce(IV) and two to Ce(III) (violet line). Two additional components of the Ce 3 $d_{5/2}$ were overlapped with the Ni $2p_{1/2}$ peaks. The support contained predominantly Ce(IV), with only about 2% of the total Ce present as Ce(III). In the Cu 2p region (Fig. S5B), the two peaks at 932.2 and 952.2 eV were consistent with the presence of Cu^{+}. Indeed, the possible presence of Cu^{2+} states is characterized by peaks at higher BE (usually at about 934 and 954 eV) [9,39]. Nevertheless, the simultaneous presence of Cu^{0} species cannot be excluded, since Cu^{0} and Cu^{+} exhibit very similar Cu 2p binding energies and spectral features [39,40]. Analysis of the Cu LMM Auger transitions would be required to discriminate between these oxidation states; however, in the present case, the Auger signal intensity was insufficient for a reliable analysis because of the very low copper oxide loading. The two bands in the Ti 2p region (Fig. S5C) are associated with the Ti^{4+} with a peak separation of about 5.9 eV, typical of the TiO_2 P25 [41].

The interaction between the modified kaolinite support and the Cu_2O-TiO_2, together with the presence of copper species, promoted a more efficient separation of photogenerated charge carriers. Indeed, the PL spectrum of 1CuTi/KAO exhibited a lower band emission intensity than that of unsupported 1CuTi, indicating a reduced electrons–holes recombination rate and a more effective charge carriers separation (Fig. S6) [42]. Three main emission bands were observed. The emission centred at approximately 433 nm can be attributed to defect states, surface oxygen vacancies, and/or exciton recombination through bulk defects [43]. The band at about 486 nm is associated with the excitonic transitions from sublevels of the conduction band, generated by the presence of the copper species, to the valence band of TiO_2. Finally, the broad emission centred at around 540 nm is likely related to surface defects in the TiO_2 crystalline structure, whose formation may be further promoted by the interaction with the modified kaolinite support [43].

Finally, the SEM-EDX analysis (Figs. S7, Table S1) of the same sample showed, in accordance with the literature, the typical heterogeneous morphology of this type of composites [7,44,45].

The proposed reaction mechanism for the CO_2 reduction, coming from the thermocatalytic oxidation of toluene, using the best sample (1CuTi/KAO) relies on the synergistic interaction of several processes contributing to solar fuels production. First, the combination of thermocatalytic and photocatalytic pathways enhances the mobility and availability of protons generated from water vapor oxidation, which is widely recognized as the rate-determining step in CO_2 photoreduction [8,46]. This synergistic effect promotes the simultaneous interaction of photogenerated electrons, protons, and adsorbed CO_2 molecules, thereby improving the overall reaction efficiency. In particular, CO_2 is efficiently adsorbed on the medium-strength basic sites of kaolinite, as evidenced by CO_2-TPD measurements. Subsequently, the adsorbed molecules are activated by the intercalated Ni and Ce species and converted into solar fuels through the cooperative action of the Cu_2O-TiO_2 composite.

Secondary, the presence of copper species, mainly attributed to Cu^{+} with a possible contribution from metallic Cu^{0}, as suggested by the XPS analysis, represents a beneficial feature for the photothermo-catalytic process. Cuprous oxide can act as an electron mediator owing to its favourable conduction band position [47], facilitating charge transfer toward the adsorbed CO_2 molecules. Moreover, the intimate interaction between Cu species and TiO_2 facilitates the charge carriers separation, limiting the electron-hole recombination as verified by the PL measurements. This increases the availability of electrons for the CO_2 reduction reaction. Metallic Cu^{0} species may further promote electron mobility and reduce the kinetic barrier associated with the CO_2 conversion reaction [48]. In this way the solar fuels formation was efficiently promoted.

The obtained results, namely a CO_2 capture efficiency of approximately 70% achieved with the zeolite 13X/chitosan/PEGDGE cryogel in the integrated test and a CO_2 conversion of 77% over the 1 wt% Cu_2O-TiO_2 composite supported on Ni/Ce-kaolinite under photothermo-catalytic conditions at 120 °C, demonstrate the potential of the proposed integrated approach. Future efforts will focus on further tuning the capture properties of the cryogel to enhance both CO_2 uptake and selectivity, while also investigating strategies to control the desorption of the captured CO_2 and its subsequent conversion into solar fuels. This approach may help overcome some of the major limitations associated with photothermo-catalytic CO_2 conversion when CO_2 originates from VOC oxidation process. Indeed, the complex gas stream, consisting of CO_2, air, water vapor and possible trace of by-products, may significantly affect catalytic activity, products distribution, and long-term catalyst stability.

Furthermore, a deeper understanding of the electronic structure and charge-transfer processes within the multicomponent Cu_2O–TiO_2/Ni/Ce-kaolinite catalyst is required. Advanced investigations including DFT calculations, Mott–Schottky analyses, and photoelectrochemical characterizations, will provide valuable insights into the electronic structure of the composite and how it can influence the catalytic performance. Such information will be crucial for guiding catalyst design and optimizing both synthesis parameters and operating conditions, ultimately leading to further improvements in CO_2 conversion efficiency and solar fuels production using an integrated air purification platform.

4. Conclusions

In this work, an integrated approach for the management of the CO_2 produced by the catalytic oxidation of toluene was investigated, combining two sustainable routes, namely CO_2 capture by zeolite-based cryogels and CO_2 conversion into solar fuels by noble metal-free photothermo-catalysts. The introduction of zeolite 13X into the chitosan/PEGDGE cryogel strongly improved the CO_2 uptake, allowing a capture efficiency of about 70% in the integrated test, whereas the cryogel without zeolite showed only a negligible capture ability. On the other hand, the 1 wt% Cu_2O-TiO_2 composite supported on Ni/Ce-modified phyllosilicates efficiently promoted the photothermo-catalytic CO_2 conversion. Among the examined samples, the utilization of the modified kaolinite showed the best performance, with 77% of CO_2 conversion and a CO and CH_4 formation rate of about 21 and 9 $\mu mol/g_{cat}\bullet h$, respectively, after 4 h of reaction at 120 °C. The improved activity of this sample was mainly related to the higher amount of basic sites, especially medium basic sites, that favoured the adsorption and activation of CO_2, whereas the Cu_2O-TiO_2 composite promoted the photocatalytic contribution under simulated solar irradiation. Therefore, the synergism between the thermocatalytic features of the modified phyllosilicates and the photocatalytic properties of Cu_2O-TiO_2 allowed to efficiently valorise the CO_2 arising from the removal of an air pollutant. The approach proposed here is promising to couple air purification with CO_2 capture/utilization using sustainable materials, thus contributing to a more circular strategy for environmental protection. At the same time, this work provides a proof-of-concept of a dual route in which the CO_2 generated from VOC removal can be managed either through capture or through conversion into solar fuels, depending on the desired application.

CRediT authorship contribution statement

Martina Salzano De Luna: Writing – review & editing, Methodology, Investigation, Formal analysis, Data curation. **Roberto Fiorenza:** Writing – review & editing, Writing – original draft, Validation, Supervision, Project administration, Investigation, Funding acquisition, Formal analysis, Data curation, Conceptualization. **Marianna Bellardita:** Writing – review & editing, Visualization, Validation, Supervision,

Methodology, Investigation. **Luca Calantropo:** Investigation, Formal analysis. **Giusy Dativo:** Investigation, Formal analysis. **Riccardo Scarfiello:** Writing – review & editing, Supervision, Methodology. **Luigi Carbone:** Writing – review & editing, Validation, Supervision, Project administration. **Mariano Sirignano:** Writing – review & editing, Methodology, Investigation, Formal analysis, Data curation.

Declaration of Competing Interest

The authors declare that they have no known competing financial interests or personal relationships that could have appeared to influence the work reported in this paper.

Acknowledgments

All the authors thank the financial support under the National Recovery and Resilience Plan (NRRP), funded by the European Union – NextGeneration EU—DD 1409 Progetti di Rilevante Interesse Nazionale (PRIN) 2022 PNRR published on 14–09–2022 by the Italian Ministry of Research (MUR), Missione 4 (Istruzione e Ricerca) Component 2, Investment in the CO2@ photothermocat project (P2022JXKKF, CUP E53D23015700001). L.C. and R.S. acknowledge also the Italian Ministry of Research (MUR) in the framework of the National Recovery and Resilience Plan (NRRP) and under the complementary actions to the NRRP funded by NextGenerationEU, "Fit4MedRob" Grant (PNC0000007, B53C22006960001). The authors also thank Sofia Virzì and Simona Didomenico for the help in the catalytic measurements.

Appendix A. Supporting information

Supplementary data associated with this article can be found in the online version at doi:10.1016/j.cattod.2026.115898

Data availability

Data will be made available on request.

References

[1] A. Aslam, X. Yu, G. Akhtar, From emissions to solutions: The role of green energy, environmental policy stringency, and political stability in achieving BRICS' carbon neutrality goals, J. Environ. Manag. 395 (2025) 127871, https://doi.org/10.1016/j.jenvman.2025.127871.

[2] J. Zhao, Y. Wang, Z. Chen, Y. Gao, T. Xue, G. Liu, S. Xin, C. Zhou, Y. Xin, Q. Wang, Q. Yan, Recent advances in catalytic removal volatile organic compounds: Structure activity correlation, mechanism and application insights, Sep. Purif. Technol. 378 (2025) 134598, https://doi.org/10.1016/j.seppur.2025.134598.

[3] S. Lawson, K. Newport, Q. Al-Naddaf, A.E. Ameh, A.A. Rownaghi, L.F. Petrik, F. Rezaei, Binderless zeolite monoliths production with sacrificial biopolymers, Chem. Eng. J. 407 (2021) 128011, https://doi.org/10.1016/j.cej.2020.128011.

[4] B. Liguori, P. Aprea, G. Roviello, C. Ferone, Self-supporting zeolites by Geopolymer Gel Conversion (GGC), Microporous Mesoporous Mater. 286 (2019) 125–132, https://doi.org/10.1016/j.micromeso.2019.05.045.

[5] L. Valencia, W. Rosas, A. Aguilar-Sanchez, A.P. Mathew, A.E.C. Palmqvist, Bio-based Micro-/Meso-/Macroporous Hybrid Foams with Ultrahigh Zeolite Loadings for Selective Capture of Carbon Dioxide, ACS Appl. Mater. Interfaces 11 (2019) 40424–40431, https://doi.org/10.1021/acsami.9b11399.

[6] G. Dativo, M. Condorelli, G. Compagnini, G. Impellizzeri, S. Scirè, R. Fiorenza, CO2 conversion by solar photothermo co-catalysis on montmorillonite-based catalysts, Discov. Appl. Sci. 7 (2025) 186, https://doi.org/10.1007/s42452-025-06622-0.

[7] G. Dativo, E. La Greca, L.F. Liotta, V. La Parola, M. Condorelli, G. Impellizzeri, G. Compagnini, S. Sciré, R. Fiorenza, Solar photothermo-catalytic conversion of CO2 on phyllosilicates modified with Ni and CeO2, J. CO2 Util. 82 (2024) 102765, https://doi.org/10.1016/j.jcou.2024.102765.

[8] R. Fiorenza, M. Bellardita, S.A. Balsamo, A. Gulino, M. Condorelli, G. Compagnini, S. Scirè, L. Palmisano, A solar photothermo-catalytic combined process for the VOCs combustion and the subsequent CO2 valorization using noble metal-free catalysts, Catal. Today 413415 (2023) 113949, https://doi.org/10.1016/j.cattod.2022.11.010.

[9] R. Fiorenza, C. Contarino, V. Spanò, M.T.A. Iapichino, S.A. Balsamo, Photothermo-catalytic strategies for the CO2 valorisation using TiO2-based composites, Catal. Today 423 (2023) 114251, https://doi.org/10.1016/j.cattod.2023.114251.

[10] B. Li, K. Zhang, X. Wang, Y. Li, X. Liu, B.-H. Han, F. Li, Construction synergetic adsorption and activation surface via confined Cu/Cu2O and Ag nanoparticles on TiO2 for effective conversion of CO2 to CH4, J. Colloid Interface Sci. 660 (2024) 961–973, https://doi.org/10.1016/j.jcis.2024.01.159.

[11] R. Fiorenza, M. Bellardita, S.A. Balsamo, L. Spitaleri, A. Gulino, M. Condorelli, L. D'Urso, S. Scirè, L. Palmisano, A solar photothermocatalytic approach for the CO2 conversion: Investigation of different synergisms on CoO-CuO/brookite TiO2-CeO2 catalysts, Chem. Eng. J. 428 (2022) 131249, https://doi.org/10.1016/j.cej.2021.131249.

[12] E. Luzzi, P. Aprea, M. Salzano de Luna, D. Caputo, G. Filippone, Mechanically Coherent Zeolite 13X/Chitosan Aerogel Beads for Effective CO 2 Capture, ACS Appl. Mater. Interfaces 13 (2021) 20728–20734, https://doi.org/10.1021/acsami.1c04064.

[13] S. Bratskaya, Y. Privar, D. Nesterov, E. Modin, M. Kodess, A. Slobodyuk, D. Marinin, A. Pestov, Chitosan Gels and Cryogels Cross-Linked with Diglycidyl Ethers of Ethylene Glycol and Polyethylene Glycol in Acidic Media, Biomacromolecules 20 (2019) 1635–1643, https://doi.org/10.1021/acs.biomac.8b01817.

[14] V. Durgakumari, M. Subrahmanyam, K.V. Subba Rao, A. Ratnamala, M. Noorjahan, K. Tanaka, An easy and efficient use of TiO2 supported HZSM-5 and TiO2 + HZSM-5 zeolite combinate in the photodegradation of aqueous phenol and p-chlorophenol, Appl. Catal. A Gen. 234 (2002) 155–165, https://doi.org/10.1016/S0926-860X(02)00224-7.

[15] P. Makuła, M. Pacia, W. Macyk, How To Correctly Determine the Band Gap Energy of Modified Semiconductor Photocatalysts Based on UV–Vis Spectra, J. Phys. Chem. Lett. 9 (2018) 6814–6817, https://doi.org/10.1021/acs.jpclett.8b02892.

[16] S. Landi, I.R. Segundo, E. Freitas, M. Vasilevskiy, J. Carneiro, C.J. Tavares, Use and misuse of the Kubelka-Munk function to obtain the band gap energy from diffuse reflectance measurements, Solid. State Commun. 341 (2022) 114573, https://doi.org/10.1016/j.ssc.2021.114573.

[17] R. Fiorenza, C. Crisafulli, G.G. Condorelli, F. Lupo, S. Scirè, Au-Ag/CeO2 and Au-Cu/CeO2 Catalysts for Volatile Organic Compounds Oxidation and CO Preferential Oxidation, Catal. Lett. 145 (2015) 1691–1702, https://doi.org/10.1007/s10562-015-1585-5.

[18] M. Dilla, R. Schlögl, J. Strunk, Photocatalytic CO 2 Reduction Under Continuous Flow High-Purity Conditions: Quantitative Evaluation of CH 4 Formation in the Steady-State, ChemCatChem 9 (2017) 696–704, https://doi.org/10.1002/cctc.201601218.

[19] A. Cornelio, A. Zanoletti, G. Dativo, R. Fiorenza, A. Zacco, M. Muhyuddin, C. Santoro, L.E. Depero, E. Bontempi, Performance and structural evolution of a new critical raw material-free catalyst, synthesized from spent lithium-ion batteries, for solar-driven CO 2 conversion, Green. Chem. 27 (2025) 10132–10144, https://doi.org/10.1039/D5GC02583D.

[20] M.A. Al-Ghouti, D.A. Da'ana, Guidelines for the use and interpretation of adsorption isotherm models: A review, J. Hazard. Mater. 393 (2020) 122383, https://doi.org/10.1016/j.jhazmat.2020.122383.

[21] K. Kawata, S. Maeda, S. Iguchi, S. Naniwa, M. Nishimoto, K. Teramura, Photocatalytic conversion of CO2 using various TiO2 modified with Ag and Co dual cocatalysts via an ultrasonic reduction method, Catal. Today 461 (2026) 115532, https://doi.org/10.1016/j.cattod.2025.115532.

[22] R. Ma, J. Sun, D.H. Li, J.J. Wei, Review of synergistic photo-thermo-catalysis: Mechanisms, materials and applications, Int. J. Hydrog. Energy 45 (2020) 30288–30324, https://doi.org/10.1016/j.ijhydene.2020.08.127.

[23] W. Zhang, D. Ma, J. Pérez-Ramírez, Z. Chen, Recent Progress in Materials Exploration for Thermocatalytic, Photocatalytic, and Integrated Photothermocatalytic CO 2 -to-Fuel Conversion, Adv. Energy Sustain. Res. 3 (2022) 2100169, https://doi.org/10.1002/aesr.202100169.

[24] V. Patamia, R. Fiorenza, I. Brullo, M. Zambito Marsala, S.A. Balsamo, A. Distefano, P.M. Furneri, V. Barbera, S. Scirè, A. Rescifina, A sustainable porous composite material based on loofah-halloysite for gas adsorption and drug delivery, Mater. Chem. Front. 6 (2022) 2233–2243, https://doi.org/10.1039/D2QM00505K.

[25] A.K. Mishra, S. Allauddin, R. Narayan, T.M. Aminabhavi, K.V.S.N. Raju, Characterization of surface-modified montmorillonite nanocomposites, Ceram. Int. 38 (2012) 929–934, https://doi.org/10.1016/j.ceramint.2011.08.012.

[26] A. Kumar, P. Lingfa, Sodium bentonite and kaolin clays: Comparative study on their FT-IR, XRF, and XRD, Mater. Today Proc. 22 (2020) 737–742, https://doi.org/10.1016/j.matpr.2019.10.037.

[27] A. Davydov. Molecular Spectroscopy of Oxide Catalyst Surfaces, Wiley, 2003, https://doi.org/10.1002/0470867981.

[28] R.W. Stevens, R.V. Siriwardane, J. Logan, In Situ Fourier Transform Infrared (FTIR) Investigation of CO 2 Adsorption onto Zeolite Materials, Energy & Fuels 22 (2008) 3070–3079, https://doi.org/10.1021/ef800209a.

[29] Y. Bao, C. Huang, L. Chen, Y.dong Zhang, L. Liang, J. Wen, M. Fu, J. Wu, D. Ye, Highly efficient Cu/anatase TiO 2 {001}-nanosheets catalysts for methanol synthesis from CO 2, J. Energy Chem. 27 (2018) 381–388, https://doi.org/10.1016/j.jechem.2017.12.015.

[30] D. Schmider, L. Maier, O. Deutschmann, Reaction Kinetics of CO and CO 2 Methanation over Nickel, Ind. Eng. Chem. Res. 60 (2021) 5792–5805, https://doi.org/10.1021/acs.iecr.1c00389.

[31] L. Calantropo, E. La Greca, L.F. Liotta, G. Impellizzeri, A. Gulino, A. Ferlazzo, L. Vitiello, S.C. Carroccio, S. Scirè, R. Fiorenza, Solar photothermo-catalytic CO2 conversion into methane: Effect of phyllosilicates on the performance of Ni-Zn-Al layered double hydroxide-derived catalysts, J. CO2 Util. 103 (2026) 103302, https://doi.org/10.1016/j.jcou.2025.103302.

[32] K. Wu, Q. Ye, R. Wu, S. Chen, H. Dai, Carbon dioxide adsorption behaviors of aluminum-pillared montmorillonite-supported alkaline earth metals, J. Environ. Sci. 98 (2020) 109–117, https://doi.org/10.1016/j.jes.2020.05.025.

[33] M. Nguyen-Quang, F. Azzolina-Jury, B. Samojeden, M. Motak, P. Da Costa, On the influence of the preparation routes of NiMgAl-mixed oxides derived from hydrotalcite on their CO2 methanation catalytic activities, Int. J. Hydrog. Energy 47 (2022) 37783–37791, https://doi.org/10.1016/j.ijhydene.2022.08.278.
[34] M. Thommes, K. Kaneko, A.V. Neimark, J.P. Olivier, F. Rodriguez-Reinoso, J. Rouquerol, K.S.W. Sing, Physisorption of gases, with special reference to the evaluation of surface area and pore size distribution (IUPAC Technical Report), Pure Appl. Chem. 87 (2015) 1051–1069, https://doi.org/10.1515/pac-2014-1117.
[35] K. Wang, Z. Bielan, M. Endo-Kimura, M. Janczarek, D. Zhang, D. Kowalski, A. Zielińska-Jurek, A. Markowska-Szczupak, B. Ohtani, E. Kowalska, On the mechanism of photocatalytic reactions on Cu x O@TiO 2 core–shell photocatalysts, J. Mater. Chem. A 9 (2021) 10135–10145, https://doi.org/10.1039/D0TA12472A.
[36] J. Li, N. Zhang, X. Sun, X. Zhou, H. Wu, Construction of Cu2O@TiO2 core-shell structure S-scheme heterojunction for efficient photoreduction CO2 into CH4: Interface engineering regulates charge transfer and CO2 adsorption, Chem. Eng. J. 522 (2025) 167515, https://doi.org/10.1016/j.cej.2025.167515.
[37] Y. Gao, A. Aihemaiti, J. Jiang, Y. Meng, T. Ju, S. Han, X. Chen, J. Liu, Inspection over carbon deposition features of various nickel catalysts during simulated biogas dry reforming, J. Clean. Prod. 260 (2020) 120944, https://doi.org/10.1016/j.jclepro.2020.120944.
[38] R. Fiorenza, S.A. Balsamo, L. D'Urso, S. Sciré, M.V. Brundo, R. Pecoraro, E. M. Scalisi, V. Privitera, G. Impellizzeri, CeO2 for Water Remediation: Comparison of Various Advanced Oxidation Processes, Catalysts 10 (2020) 446, https://doi.org/10.3390/catal10040446.
[39] S. Poulston, P.M. Parlett, P. Stone, M. Bowker, Surface Oxidation and Reduction of CuO and Cu2O Studied Using XPS and XAES, Surf. Interface Anal. 24 (1996) 811–820, https://doi.org/10.1002/(SICI)1096-9918(199611)24:12<811:AID-SIA191>3.0.CO;2-Z.
[40] Y. Zheng, L. Zhang, J. Guan, S. Qian, Z. Zhang, C.K. Ngaw, S. Wan, S. Wang, J. Lin, Y. Wang, Controlled Synthesis of Cu 0 /Cu 2 O for Efficient Photothermal Catalytic Conversion of CO 2 and H 2 O, ACS Sustain. Chem. Eng. 9 (2021) 1754–1761, https://doi.org/10.1021/acssuschemeng.0c07702.
[41] B. Erdem, R.A. Hunsicker, G.W. Simmons, E.D. Sudol, V.L. Dimonie, M.S. El-Aasser, XPS and FTIR Surface Characterization of TiO 2 Particles Used in Polymer Encapsulation, Langmuir 17 (2001) 2664–2669, https://doi.org/10.1021/la0015213.
[42] J. Liqiang, Q. Yichun, W. Baiqi, L. Shudan, J. Baojiang, Y. Libin, F. Wei, F. Honggang, S. Jiazhong, Review of photoluminescence performance of nano-sized semiconductor materials and its relationships with photocatalytic activity, Sol. Energy Mater. Sol. Cells 90 (2006) 1773–1787, https://doi.org/10.1016/j.solmat.2005.11.007.
[43] K. Sabzehei, S.H. Hadavi, M.G. Bajestani, S. Sheibani, Comparative evaluation of copper oxide nano-photocatalyst characteristics by formation of composite with TiO2 and ZnO, Solid. State Sci. 107 (2020) 106362, https://doi.org/10.1016/j.solidstatesciences.2020.106362.
[44] M. Darder, E. Ruiz-Hitzky, Caramel–clay nanocomposites, J. Mater. Chem. 15 (2005) 3913, https://doi.org/10.1039/b505958e.
[45] E. Manova, P. Aranda, M. Angeles Martín-Luengo, S. Letaïef, E. Ruiz-Hitzky, New titania-clay nanostructured porous materials, Microporous Mesoporous Mater. 131 (2010) 252–260, https://doi.org/10.1016/j.micromeso.2009.12.031.
[46] S. Fang, Y.H. Hu, Thermo-photo catalysis: a whole greater than the sum of its parts, Chem. Soc. Rev. (2022) 3609–3647, https://doi.org/10.1039/d1cs00782c.
[47] S. Ali, J. Lee, H. Kim, Y. Hwang, A. Razzaq, J.W. Jung, C.H. Cho, S.Il In, Sustained, photocatalytic CO2 reduction to CH4 in a continuous flow reactor by earth-abundant materials: Reduced titania-Cu2O Z-scheme heterostructures, Appl. Catal. B Environ. 279 (2020) 119344, https://doi.org/10.1016/j.apcatb.2020.119344.
[48] H. Xie, J. Wang, K. Ithisuphalap, G. Wu, Q. Li, Recent advances in Cu-based nanocomposite photocatalysts for CO2 conversion to solar fuels, J. Energy Chem. 26 (2017) 1039–1049, https://doi.org/10.1016/j.jechem.2017.10.025.